Geophysical Journal International

Geophys. J. Int. (2024) **239,** 70–84
Advance Access publication 2024 July 22
GJI Applied and Marine Geophysics
https://doi.org/10.1093/gji/ggae254

Quantifying the mineral magnetic signature of petroleum systems and their source rocks: a study on the Inner Moray Firth, UK North Sea

J.R. Perkins,[1] A.R. Muxworthy,[1,2] A.J. Fraser[1] and P. Hu[3]

[1]*Department of Earth Science and Engineering, Imperial College London, London SW7 2BP, UK. E-mail: j.perkins18@imperial.ac.uk*
[2]*Department of Earth Sciences, University College London, London WC1E 6BS, UK*
[3]*Research School of Earth Sciences, Australian National University, Acton ACT 0200, Australia*

Accepted 2024 July 18. Received 2024 July 16; in original form 2023 June 14

SUMMARY

This study aims to expand on existing connections between magnetic minerals and hydrocarbons within petroleum systems. Previous studies have focussed on single-source petroleum systems whereas this study, for the first time, analyses a multi-source petroleum system to investigate potential correlations between different kerogen type source rocks and magnetic minerals. To do this, the study investigates the magnetic mineral characteristics of the Inner Moray Firth (IMF), UK North Sea, through room-, low- and high-temperature techniques, and correlates this to published basin and petroleum systems modelling results that show a three-source hydrocarbon mix. Magnetic mineral analysis identifies extensive evidence for magnetite, goethite and siderite, alongside more minor lepidocrocite and iron sulphides. Although we find that magnetite is ubiquitous within the IMF, its abundance is relatively low, and, in contrast, the relatively magnetically weak goethite is more likely the most abundant magnetic mineral throughout the IMF. In agreement with previous studies, we find magnetic enhancement at oil-water contacts (OWCs); however, here, we identify two different magnetic enhancement processes at OWCs in wells, which are dependent on the amount of sulphur available in the local environment. Wells with low levels of sulphur have increasing levels of magnetite towards the OWC, with the magnetic enhancement occurring at the top of the water-saturated section. Sulphur-rich environments display an increase in iron sulphides near the OWC at the bottom of the oil-saturated sediments. Additionally, we confirm the presence of siderite as indicator of upward vertical migration. Combining with petroleum system model predictions, we find direct links between iron hydroxide presence and Type I and II–III kerogen source rocks, and iron sulphide presence with Type II kerogen source rocks. This study shows the potential for further utilization of magnetic mineral analysis within hydrocarbon exploration and petroleum system definition.

Key words: Magnetic mineralogy and petrology; Marine magnetics and palaeomagnetics; Rock and mineral magnetism; Ocean drilling.

1 INTRODUCTION

The Inner Moray Firth (IMF), UK North Sea (Fig. 1), has a functioning but poorly understood petroleum system—there is no clear consensus as to which organic matter-rich formations mature, generate and charge the system (Linsley *et al.* 1980; Brown *et al.* 1988; Peters *et al.* 1989; Andrews *et al.* 1990; Greenhalgh 2016). This relatively poor understanding of the IMF is a consequence of limited successes during early-stage hydrocarbon exploration. However, some knowledge is present, for example the IMF petroleum system is geologically distinct from other regions in the North Sea (Andrews *et al.* 1990).

It is the aim of this paper, alongside its companion paper (Perkins *et al.* 2023), to improve our understanding of the petroleum system within the IMF, and petroleum systems in general. Using basin and petroleum systems modelling (BPSM), Perkins *et al.* (2023) showed that several formations in the IMF are effective source rocks that generate and expel hydrocarbons (Fig. 2). These source rocks are: (1) the Type I kerogen-bearing, lacustrine Devonian Fish Beds; (2) Type II-III kerogen-bearing, lagoonal and shallow marine Middle Jurassic Pentland Formation and (3) the Type II kerogen-bearing, deep marine Kimmeridge Clay black shales (Perkins *et al.* 2023). BPSM of Perkins *et al.* (2023) predicts that the Kimmeridge Clay source rocks, which are the dominant hydrocarbon source in other

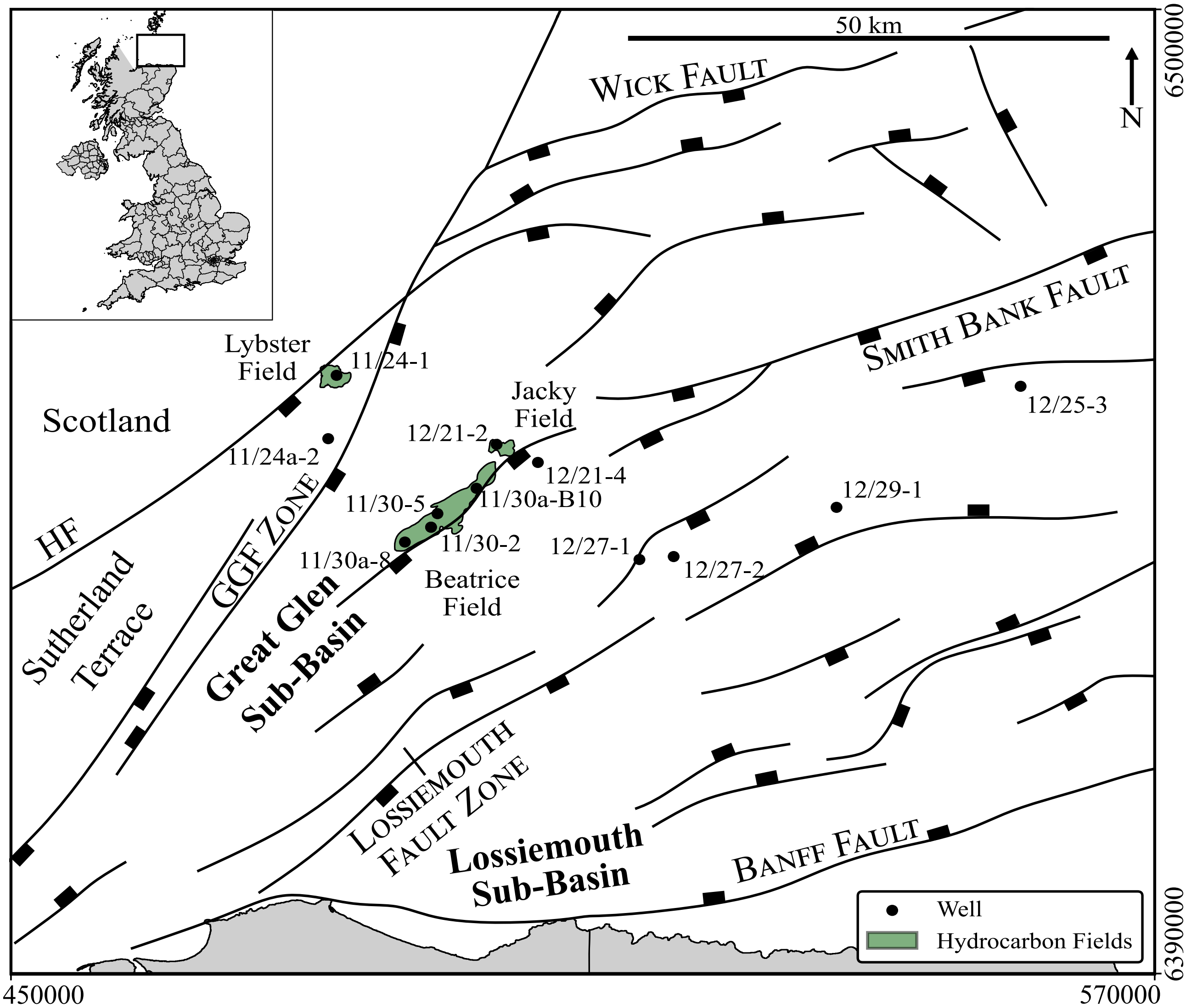

Figure 1. Structural map of the IMF showing the hydrocarbon fields and well sample locations. GGF, Great Glen Fault; HF, Helmsdale Fault. Map from Perkins *et al.* (2023), modified from Linsley *et al.* (1980) and Roberts *et al.* (1990). Note that the coordinate system is WGS 84/UTM 30N.

regions of the North Sea, are mostly too shallow to generate large volumes of hydrocarbons within the IMF. BPSM also suggested that both vertical and lateral migration of hydrocarbons occurs basin-wide (Perkins *et al.* 2023). Given that it has been demonstrated that mineral magnetic methods are able to distinguish between vertical and lateral migration (Badejo *et al.* 2021a; Abdulkarim *et al.* 2022a), in this paper we apply these magnetic methods to constrain and test the petroleum system model predictions of Perkins *et al.* (2023).

Research has shown that the presence of hydrocarbons alters the magnetic signature of rocks (Elmore *et al.* 1987; Elmore & Crawford 1990). The magnetic minerals in the rocks can alter as a direct result of the reducing effect of hydrocarbons themselves, or other processes, for example biodegradation of the oil (Elmore *et al.* 2012). These changes to the magnetic signature can be attributed either to the generation of new magnetic minerals, or the destruction or alteration of pre-existing ones (Machel 1995; Emmerton *et al.* 2013). In effect, as hydrocarbons migrate through a system they act as a diagenesis front altering the magnetic signature of the rocks that they pass through. These changes can be exploited to understand hydrocarbon migration (Abubakar *et al.* 2020; Abdulkarim *et al.* 2022b). For example, siderite has been found to form in the presence of upwardly migrating hydrocarbons (Badejo *et al.* 2021a; Abdulkarim *et al.* 2022a), and magnetic enhancements have been observed at OWCs (Badejo *et al.* 2021b; Abdulkarim *et al.* 2022c). Research has also shown that magnetic minerals are formed during hydrocarbon generation (Abubakar *et al.* 2015), though it is uncertain if these neo-formed magnetic minerals freely migrate with the hydrocarbons. This study uses variations in magnetic mineral assemblages in the IMF to better constrain and understand this petroleum system.

2 GEOLOGICAL SETTING

2.1 Basin formation

The IMF forms the western arm of the trilete North Sea Rift (Fig. 1) and underwent several periods of instability between its opening in the Permian to its stabilization in the Cretaceous (Andrews *et al.* 1990; Roberts *et al.* 1990; Underhill 1991; Perkins *et al.* 2023). The IMF sits above the Orcadian Basin and contains the Great Glen and

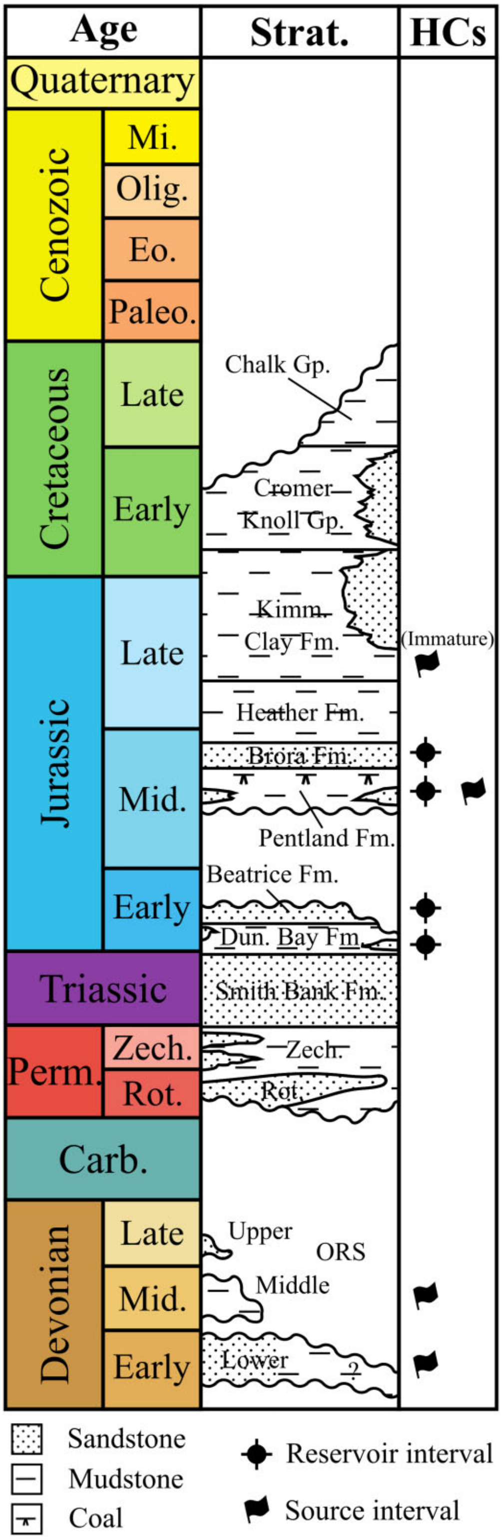

Figure 2. Stratigraphic column showing the main sedimentary and stratigraphic bodies from west to east of the Inner to Outer Moray Firths, and the key components of the petroleum system. Strat., Stratigraphy; HCs, hydrocarbon system components; Fm., Formation; Gp., Group; Kimm. Clay, Kimmeridge Clay; Dun. Bay, Dunrobin Bay; Zech., Zechstein; Rot., Rotliegend; ORS, Old Red Sandstone. From Perkins *et al.* (2023), modified from Glennie *et al.* (2003), Harker & Rieuf (1996), Peters *et al.* (1989), Stevens (1991), Underhill & Partington (1993) and Whitbread & Kearsey (2016).

Lossiemouth Sub-Basins (Andrews *et al.* 1990; Roberts *et al.* 1990; Perkins *et al.* 2023). The IMF is fault bound, being constrained to the north by the Helmsdale and Wick Faults, the Great Glen Fault to the northwest and the Banff Fault to the south (Fig. 1, Andrews *et al.* 1990; Roberts *et al.* 1990; Perkins *et al.* 2023).

The IMF evolved differently to the other arms of the North Sea Rift, despite being structurally related (Andrews *et al.* 1990; Roberts *et al.* 1990; Perkins *et al.* 2023). Following sediment deposition infilling the Orcadian Basin, the first IMF-forming event occurred as inversion and half-graben block rotation in the Early Permian to Late Triassic (Andrews *et al.* 1990; Roberts *et al.* 1990; Perkins *et al.* 2023). The second phase comprised extension of basin-bounding faults in the Jurassic–Early Cretaceous and resulted in tectonic subsidence (Andrews *et al.* 1990; Roberts *et al.* 1990; Hillis *et al.* 1994; Perkins *et al.* 2023). The third phase consisted of Early Cretaceous–Cenozoic epeirogenic subsidence, and the fourth phase was defined by uplift and erosion, caused by crustal flexure, in the Cenozoic (Andrews *et al.* 1990; Roberts *et al.* 1990; Hillis *et al.* 1994; Perkins *et al.* 2023). Beyond this four-phase basin evolution, there is evidence for two further basin-impacting events, resulting in thermal subsidence and extensional faulting (Andrews *et al.* 1990; Underhill & Partington 1993; Perkins *et al.* 2023). The first of these events followed deflation of the North Sea Thermal Dome, and the second resulted from the Late Cretaceous–Cenozoic uplift (Andrews *et al.* 1990; Underhill & Partington 1993; Perkins *et al.* 2023). Faulting in the IMF occurred predominantly syn-sedimentation, with the basin dominated by tilted fault blocks and oblique-slip faults (Roberts *et al.* 1990; Thomson & Hillis 1995; Perkins *et al.* 2023).

2.2 Basin stratigraphy

The IMF contains Devonian to Cretaceous sediments, but lacks Carboniferous intervals, all deposited syn- or post-upper crustal stretching (Andrews *et al.* 1990; Roberts *et al.* 1990; Perkins *et al.* 2023). Unconformably overlying basement metasediments and granites of the Orcadian Basin are the Devonian Lower, Middle and Upper Old Red Sandstones (ORS; Fig. 2, Andrews *et al.* 1990; Brown *et al.* 1988; Perkins *et al.* 2023), of which, the Lower ORS contains locally variable and isolated, lacustrine-deposited siltstones and mudstones (Brown *et al.* 1988; Perkins *et al.* 2023). Complete removal of previously deposited Carboniferous sands occurred in the Early Permian as a result of fault activity and extensive erosion (Andrews *et al.* 1990; Whitbread & Kearsey 2016; Perkins *et al.* 2023).

Red bed sandstones and claystones dominate the Rotliegend in the IMF, with the thin (sub-5 m-thick) Kupferschiefer Member defining its uppermost boundary (Fig. 2, Brown *et al.* 1988; Andrews *et al.* 1990; Perkins *et al.* 2023). The Zechstein deposits above the Kupferschiefer in the IMF formed in a carbonate-sulphate platform adjacent to a deep hypersaline basin, resulting in dominant clastic and carbonate sediments intermixed with anhydrite and halite (Brown *et al.* 1988; Perkins *et al.* 2023). Unconformably overlying the Zechstein are the Triassic sequences, which are predominantly mixed fine-coarse sandstones and minor siltstones, topped with the Stotfield Cherty Rock, an approximately 10 m-thick micritic carbonate sequence that contains microcrystalline silica- and sand-grain bearing chert (Brown *et al.* 1988; Perkins *et al.* 2023).

The IMF's hydrocarbon reservoir sequences are within its Jurassic sediments, and are divided into five sand bodies in four formations (Fig. 2). The oldest of these four formations are the alluvial flood basin and levee-crevasse deposits of the 'J Sand' in the Dunrobin Bay Formation, which consist of dominant fine-grained, partially cemented silty sandstones, interspersed with sandy siltstones and shales and topped by the Lady's Walk Shale, a transgressive, calcareous mudstone (Linsley *et al.* 1980; Stevens 1991; Perkins *et al.* 2023). The Beatrice Formation sits above the Dunrobin Bay Formation, and contains the 'H' and 'I' Sands that were deposited in a high energy, regressive, sandstone-dominated deltaic sequence (Linsley *et al.* 1980; Perkins *et al.* 2023). The Pentland Formation overlies the Beatrice Formation, and is a cyclical sequence of alluvial flood plain-deposited sandstones and siltstones, and flood basin-levee crevasse-deposited carbonaceous mudstones, the former of which acts as a reservoir sequence, and the latter of which acts as a source rock in the region (Linsley *et al.* 1980; Stevens 1991; Perkins *et al.* 2023). The lagoonal-coastal swamp-deposited Brora Coal, another source rock, tops the Pentland Formation (Richards *et al.* 1993). Above the Pentland Formation are the main IMF reservoir sands, contained within the Brora Formation (Linsley *et al.* 1980; Stevens 1991; Perkins *et al.* 2023). The cross-bedded, beach or barrier-deposited upper 'A' and lower 'B' Sands are divided by the mudstone-dominated Mid Shale (Linsley *et al.* 1980; Stevens 1991; Perkins *et al.* 2023). Above the Brora Formation is the reservoir-sealing Heather Formation, which contains a thin sandstone that rapidly transitions into shelf muds (Linsley *et al.* 1980; Stevens 1991; Perkins *et al.* 2023).

The Kimmeridge Clay Formation overlies the Heather Formation, and contains a sequence of highly organic-rich black shales, considered the most effective source rocks across the North Sea, and mudstones (Harker & Rieuf 1996; Whitbread & Kearsey 2016; Perkins *et al.* 2023). This fine-grained material is capped by the turbidite-deposited Wick Sand, which, in turn, is overlain by the Cromer Knoll Group (Brown *et al.* 1988; Harker & Rieuf 1996; Whitbread & Kearsey 2016; Perkins *et al.* 2023). The Cromer Knoll Group is a mix of calcareous mudstones and marls, mudstone-rich carbonates, and silts, sands and sandy marls, and, due to the Cenozoic uplift, is the most surficial formation in the IMF, bar very minor overlaying Quaternary sediments (Brown *et al.* 1988; Andrews *et al.* 1990; Perkins *et al.* 2023).

3 METHODOLOGY

3.1 Sampling and processing

Samples were collected from the British Geological Survey Core Store, Keyworth, UK. Samples were selected based on maximizing the spread of samples across all reservoir intervals whilst also focussing sampling around critical areas like OWCs (Badejo *et al.* 2021b). To do this, composite well logs were used to initially identify the stratigraphy present in each well and then to determine an interval's relevance to the petroleum system.

A total of 306 samples were taken from 12 wells (Table 1), typically between 2 and 7 cm in size, at intervals of 1 m in reservoir sections and at sub-30 cm intervals in critical areas. Note that depths in North Sea logging are conventionally in feet not metres, with this being reflected in the sample naming in this study. The sample distribution is heavily dependant on core availability, resulting in a heavy sample skew towards the reservoir sandstone intervals. All samples that were structurally strong enough were cored into 5 mm diameter cores and then trimmed to 1 cm length. Samples not suitable for coring were ground in a quartz mortar and pestle. All samples were then weighed before analysis for mass normalization.

3.2 Laboratory methods

Room-temperature hysteresis measurements were undertaken with a Princeton Measurements Vibrating Sample Magnetometer (VSM) at Imperial College London, to help determine magnetic mineral grain size and mineralogy within samples. From magnetic analysis, the saturation magnetization (M_s), remanent magnetization (M_{rs}), coercivity (B_c) and high-field susceptibility (X_{hf}) were extracted. Backfield curve analysis was measured to determine the remanent coercivity (B_{cr}).

Low-temperature measurements were carried out on a Quantum Design Magnetic Property Measurement System (MPMS) at the University of Minnesota's Institute of Rock Magnetism (I.R.M.). Low temperatures (10–300 K) are used to identify nanometric particles ($\leq$30 nm) that are hard to identify at room temperature (Dunlop & Özdemir 1997), and to identify magnetic minerals that display crystallographic transitions, for example the Verwey transition within magnetite at 120–125 K (Verwey 1939), the Morin transition in hematite at 263 K (Morin 1950), and the Besnus transition in monoclinic pyrrhotite at 30–34 K (Besnus & Meyer 1964). Three low-temperature magnetization sequences were run on the MPMS: (1) low-temperature cycling, where samples were subjected to a strong applied field at 300 K, cooled to 20 K and warmed back to 300 K in a zero-field; (2) field cooled (FC) and (3) zero-field cooled (ZFC) warming curves, where an applied field produces an SIRM at 10 K, and then is warmed in a zero-field to 300 K. These two later analyses differ through how the SIRM is reached—FC scenarios cool the sample whilst subjecting it to an applied field of 2.5 T, whereas ZFC scenarios cool the sample to 10 K in a near zero field.

Mössbauer spectroscopy was carried out on an SEE Co. Mössbauer Spectrometer at the I.R.M., at both room and low (5 and 20 K) temperatures to assess mineral assemblages in the samples. Analysis was conducted within the established MOESALZ fortran programme. Due to the very low concentrations of magnetic minerals in the samples, that is ~100 PPM, the samples were magnetically separated for Mössbauer spectroscopy, Scanning Electron Microscopy (SEM) and Energy Dispersive X-ray (EDX) analsysis, using a Frantz LB-1 Magnetic Barrier Laboratory Separator at Imperial College London. The samples were run through the separator three times to refine the volume of magnetic material. The magnetic grains were then crushed again as per Section 3.1 to ensure as fine a texture as possible.

High-temperature susceptibility measurements were carried out using an AGICO Kappabridge system at Imperial College London. Susceptibility is used to determine the mineralogy of samples based on their thermomagnetic behaviour (Muxworthy *et al.* 2023). Samples were heated from room temperature to 700 °C in an argon atmosphere, with a heating rate of 13.7 °C min^{-1}, in a field of 200 A m^{-1} and a frequency 976 Hz.

3.2.1 Scanning electron microscopy and energy dispersive X-ray analysis

For SEM analysis we used the same magnetic extraction procedure as used for the Mössbauer spectroscopy analysis on subsamples. These subsamples were then mounted on microscopy stubs and coated with chromium. SEM imaging and EDX analysis were carried out in the Centre for Electron Microscopy, Imperial College London, using a Zeiss Auriga Cross Beam system, which operates between 100 V and 30 kV, resulting in spatial resolutions of 1.0 nm and has imaging resolution to 2.5 nm.

Table 1. Arithmetic-mean magnetic results from wells in the IMF, delineated by saturating fluid (oil or water). Also included are associated hydrocarbon fields, the number of samples studied per well, the saturation magnetization (M_s), the remanent saturation magnetization (M_{rs}), the ratio M_{rs}/M_s, the coercivity (B_c), the remanent coercivity (B_{cr}), the ratio B_c/B_{cr}, the high-field susceptibility (X_{hf}) and the magnetic minerals identified through high-temperature susceptibility, low-temperature MPMS analysis, and Mössbauer spectroscopy. These are listed in order of presence from greatest to smallest. Results of each well are grouped across all formations sampled, so results are a function of the magnetic mineral assemblage across the entire section, thus are skewed to the most magnetic formations. Note: all depths presented are in measured depth, not vertical depth and Well 11/30a-B10 is a deviated well. O, oil; W, water; goe, goethite; FeS, iron sulphides; lep, lepidocrocite; mag, magnetite; mgh, maghemite; sid, siderite.

Well	Field	Depth range (ft)	Fluid	Number of samples	M_s (10^{-3} Am^2 kg^{-1})	M_{rs} (10^{-3} Am^2 kg^{-1})	M_{rs}/M_s	B_c (mT)	B_{cr} (mT)	B_{cr}/B_c	χ_{hf} (10^{-3} m^3 kg$-^1$)	Minerals identified
11/24-1	Lybster	4894-5016	O	20	2.2	0.11	0.05	4.2	58	14	9.7	mag, goe
			W	8	1.5	0.10	0.07	5.3	50	10	11	mag, goe, sid
11/24a-2	–	6090-6163	O	11	13	0.48	0.04	2.4	54	23	8.5	mag, FeS, goe
			W	5	18	0.60	0.03	2.6	62	25	20	mag, goe, sid
11/30-2	Beatrice	6343-7165	O	4	1.4	0.11	0.10	7.1	78	20	0.8	mag, goe
			W	14	1.9	0.13	0.10	6.4	64	14	76	mag, goe, sid, lep
11/30-5	Beatrice	7232-7323	O	0	–	–	–	–	–	–	–	–
			W	9	0.27	0.01	0.12	9.6	61	11	−4.8	goe, mag, lep
11/30a-8	Beatrice	6796-7075	O	8	0.90	0.07	0.09	5.3	35	7.4	21	goe, mag, sid lep
			W	25	0.78	0.06	0.15	7.6	36	5.5	9.2	goe, mag, sid, lep, FeS
11/30a-B10	Beatrice	8077-8498	O	14	1.1	0.09	0.11	6.5	41.9	7.6	−5.2	mag, goe, lep
			W	18	0.61	0.04	0.13	7.2	43	7.0	15	mag, goe, sid, lep, FeS
12/21-2	Jacky	7021-7279	O	17	3.1	0.15	0.05	3.2	52	17	1.4	mag, sid, goe, lep
			W	16	4.7	0.20	0.05	3.4	66	20	28	mag, sid, goe, lep
12/21-4	Jacky	6752-6812	O	0	–	–	–	–	–	–	–	–
			W	11	2.7	0.13	0.05	4.2	59	15	12	mag, goe, lep
12/25-3	–	4517-5630	O	14	1.4	0.18	0.13	8.4	49	5.8	3.7	mag, goe, sid
			W	6	0.89	0.07	0.08	5.8	57	9.8	−0.1	mag, goe, sid, FeS
12/27-1	–	3656-3774	O	15	1.3	0.13	0.11	7.0	60	11	51	mag, goe, sid, mgh
			W	4	2.2	0.17	0.09	6.3	52	8.8	1.7	mag, goe, mgh
12/27-2	–	5190-5224	O	8	0.78	0.08	0.11	8.8	83	12	91	goe, mag, sid, lep
			W	4	2.9	0.16	0.07	5.7	63	14	57	mag, sid, goe
12/29-1	–	6882-6929	O	7	5.2	0.32	0.06	5.4	65	12	19	mag, goe
			W	3	4.8	0.25	0.05	4.5	61	14	18	mag, goe

4 RESULTS

To constrain the magnetic mineral signature within the IMF, room-temperature magnetic analytical techniques were carried out on 306 samples. Not all samples underwent high- and low-temperature analysis due to limitations on MPMS instrument access and Kappabridge sensitivity. High-temperature susceptibility analysis was conducted on 271 samples across the twelve wells. Low-temperature analysis was conducted on 28 samples from Wells 11/24-1, in Lybster Field, 11/30-2, 11/30-5, 11/30a-8 and 11/30a-B10 in Beatrice Field, and 12/21-2 in Jacky Field, with analysis predominantly focused around the OWCs of wells within the hydrocarbon fields. In this study, we refer to relative abundance of magnetic minerals. This is because true abundance and relative mass or volume of magnetic content compared to the whole sample is difficult to accurately capture. Relative abundance in this study is classified through the ratio of the number of samples containing a magnetic mineral to the total number of samples within each well.

4.1 Room-temperature magnetic analysis

Average hysteresis parameter data is shown in Table 1 and ratioed parameters in a 'Dunlop-Day plot' in Fig. 3(a) (Day *et al.* 1977; Dunlop 2002). Generally, most samples display M_s values in the range 0.5–5 $\times 10^{-3}$ Am^2 kg^{-1}. The hysteresis parameters are indicative of large pseudo-single domain (PSD) to multidomain (MD) material; however, the position on the Day plot may also be influenced by very small superparamagnetic grains (Dunlop & Özdemir 1997). There is no clear difference between oil-saturated and water-wet

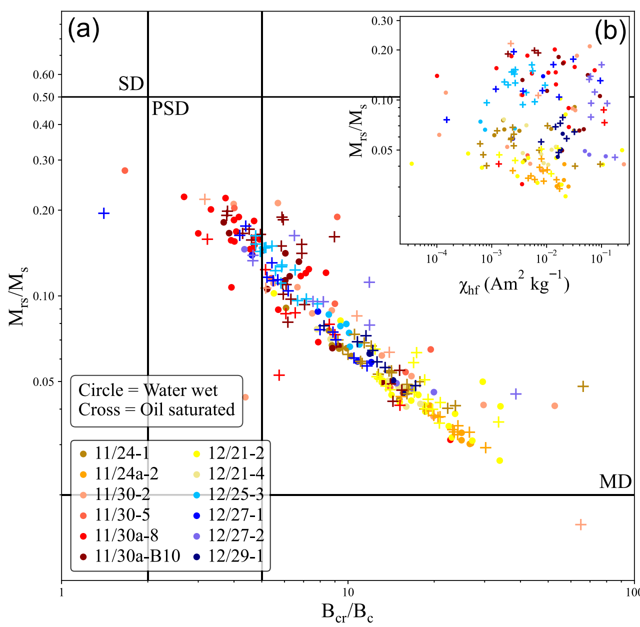

Figure 3. (a) A 'Dunlop-Day plot' (Day *et al.* 1977; Dunlop 2002) of M_{rs}/M_s against B_{cr}/B_c and (b) (inset) plot of M_{rs}/M_s against χ_{hf}, for all the samples from wells across the IMF, separated into oil-saturated (cross) and water-saturated (circle) samples. The magnetic domain state regions (single domain (SD), pseudo-SD (PSD) and multidomain (MD) are depicted in plot a, based on the Dunlop-Day plot boundaries.

samples. χ_{hf} provides a rough estimate of the level of paramagnetic material (Fig. 3b), and has been used as a tentative proxy for siderite (Abdulkarim *et al.* 2022c).

In the northwest of the IMF, Well 11/24-1 in Lybster Field and the neighbouring Well 11/24a-2 (Fig. 1) show contrasting behaviours. Well 11/24-1 shows similar M_s and M_{rs} between saturating fluids, which are broadly consistent with most studied wells, as shown through averaged data (Table 1). In contrast, Well 11/24a-2 displays the highest concentration of magnetic minerals in the whole basin. The domain state hysteresis parameters indicate that Well 11/24a-2 is also more MD-like than most samples within the study. This is shown by the coercivity (B_c) which is the lowest of all wells, whilst the remanent coercivity (B_{cr}) is average, producing the highest B_{cr}/B_c ratio across all wells (Fig. 3). The atypical magnetic response seen in Well 11/24a-2 compared to the majority of wells within the IMF suggests that a localized variation occurs within this region, along the edge of the Great Glen Fault (Fig. 1; Table 1).

The wells in the central IMF Beatrice Field, that is Wells 11/30-2, 11/30-5, 11/30a-8 and 11/30a-B10, all show broadly similar results, on average (Table 1). However, Wells 11/30a-8 and 11/30a-B10 both have much lower B_{cr}, and therefore lower B_{cr}/B_c ratios, than Wells 11/30-2 and 11/30-5, on average (Table 1). This is likely caused by a lower sampling density resulting in an increased likelihood of lithological variation not being encapsulated in the averaging of results. Although wells often show overlap, the samples from 11/30a-8 and 11/30a-B10 broadly display the most PSD-like behaviour across the IMF in Fig. 3. In contrast, the two wells from the neighbouring Jacky Field region, 12/21-2 and 12/21-4, broadly display the most MD-like signature of all the samples in the central and eastern IMF.

Across the eastern-IMF wells, the magnetic responses are all broadly similar (Table 1). The wells, 12/25-3, 12/27-1, 12/27-2 and 12/29-1, all have consistent magnetic results bar those seen within X_{hf} responses, where the oil-saturated samples consistently yield higher X_{hf} values than the water-saturated samples. This trend is not matched in the central or northern wells, with only Well 11/30a-8 having oil-saturated samples producing greater X_{hf} responses than the water-saturated ones.

Within individual wells across the IMF, magnetic enhancement can be found at the majority, albeit small, of OWCs via the increase of room-temperature M_s (Fig. 4). Of the 12 wells analysed, 10 contain both oil- and water-saturated samples, and thus all of these wells contain OWCs. The two wells that do not contain oil-saturated samples are Wells 11/30-5 in the Beatrice Field, and 12/21-4 to the south-east of Beatrice Field. Of the 10 OWC-bearing wells, nine show clear M_s enhancement at the contacts, most well-defined in Wells 11/24-1, 12/21-2 and 12/27-1 (Fig. 4).

4.2 Magnetic mineral identification

We used a range of methods to identify the magnetic minerals within out samples. High-temperature susceptibility analysis was conducted on 271 of the 306 samples, with the magnetic hysteresis measurements described above conducted on all 306 samples. Other methods were used to corroborate the high-temperature susceptibility data for selected samples.

High-temperature susceptibility analysis identified six common magnetic minerals across the samples (Fig. 5): magnetite (Fe_3O_4), goethite (α-FeOOH), siderite ($FeCO_3$), pyrite (FeS_2), lepidocrocite (γ-FeOOH) and maghemite (γ-Fe_2O_3). These interpretations are based on a wide range of literature (Housen 1996; Minyuk 2011, 2013; Badejo *et al.* 2021a; Abdulkarim *et al.* 2022a, b, c; Muxworthy *et al.* 2023). From the high-temperature susceptibility data, magnetite is identified in nearly all samples across the IMF, whilst goethite is identified in a high number of samples (Table 1; Fig. 4). In comparison, siderite is identified more often in the wells in hydrocarbon fields, but is also present in the majority of wells (nine of twelve), and lepidocrocite in just over half of wells (seven of twelve; Table 1). In contrast, iron sulphides are only present in four of the analysed wells, and was most common in Well 11/24a-2 (Table 1; Fig. 4). High-temperature susceptibility identified changes in the magnetic mineral presence around the oil–water contacts (Fig. 4). (1) The iron hydroxides goethite and lepidocrocite were typically identified above the oil–water contacts and less frequently, although still present, below; (2) siderite is predominantly identified away from OWCs, but is identified adjacent to, and across, OWCs in two wells and (3) magnetite was frequently identified in both oil- and water-saturated regions.

To corroborate the the high-temperature susceptibility analysis, low-temperature measurements were made (Fig. 6). In these measurements the Verwey transition of magnetite was observed in all samples, for example in Well 11/30a-8. Given the relative spontaneous magnetizations of goethite and magnetite (Dunlop & Özdemir 1997), it only requires relatively low concentrations of magnetite for it to dominate the magnetic signature of an assemblage. We have also identified siderite and goethite in some of the water-saturated samples. That is, the low-temperature data supports the high-temperature susceptibility data.

We found both increased magnetite presence and a decrease in goethite towards the OWC, from both the water- and oil-saturated regions, that is on approaching the OWC from both above and below, suggesting the alteration of goethite to magnetite at and near the OWC, akin to the decrease in siderite towards the OWC as shown in Fig. 6. This mechanism would give rise to the general increase in magnetization towards the oil-water contacts (Fig. 4).

Mössbauer spectroscopy was conducted on three samples from Well 11/30a-8 (7019 ft, 7021 ft and 7024 ft; Fig. 7). All Mössbauer spectra either show the same behaviour as Fig. 7 or did not produce definitive results. Even at 5 K, the Mössbauer spectra have no evidence for ferromagnetic (*s.l.*) sextets with only doublets observed, that is no evidence for magnetite, siderite below its Néel temperature, etc. (Vandenberghe 1986; Ristic 2017), although ferromagnetic phases were routinely observed magnetically (e.g. Figs 3 and 6). This is likely due to the paramagnetic phases dominating the ferromagnetic signals with this method, and may be related to preferential extraction of paramagnetic minerals via the Frantz. Two doublets are fitted to the spectra measured at 5 K for a sample from well 11/30a-8 (Fig. 7). The isomer shift (IS) and quadrupole splitting (QS) values of Doublet 1 are similar to paramagnetic iron sulphides, mostly likely to be pyrite (Evans 1982; Kar 2004), however, this is inconsistent with the high-temperature susceptibility and SEM/EDX analysis that show no presence of iron sulphides in the samples. Doublet 2 is most likely ankerite ($CaFe(CO_2)_3$) which is chemically similar to siderite, but has a lower QS values and importantly does not display long-range ordering at 1.7 K, that is it is paramagnetic at 5 K (Hilscher *et al.* 2005; Vandenberghe & de Grave 2013). The QS value for this sample at room-temperature is 1.47 mm s^{-1} (Perkins 2022); published QS values for ankerite are 1.44–1.48 mm s^{-1} (Reeder & Dollase 1989) and siderite 1.79 mm s^{-1} (Vandenberghe & de Grave 2013). Siderite and ankerite often coexist, as they are crystallographically related (Hilscher *et al.* 2005), with ankerite forming within hydrocarbon source shales as a result of clay mineral diagenesis (Kantorowicz 1985).

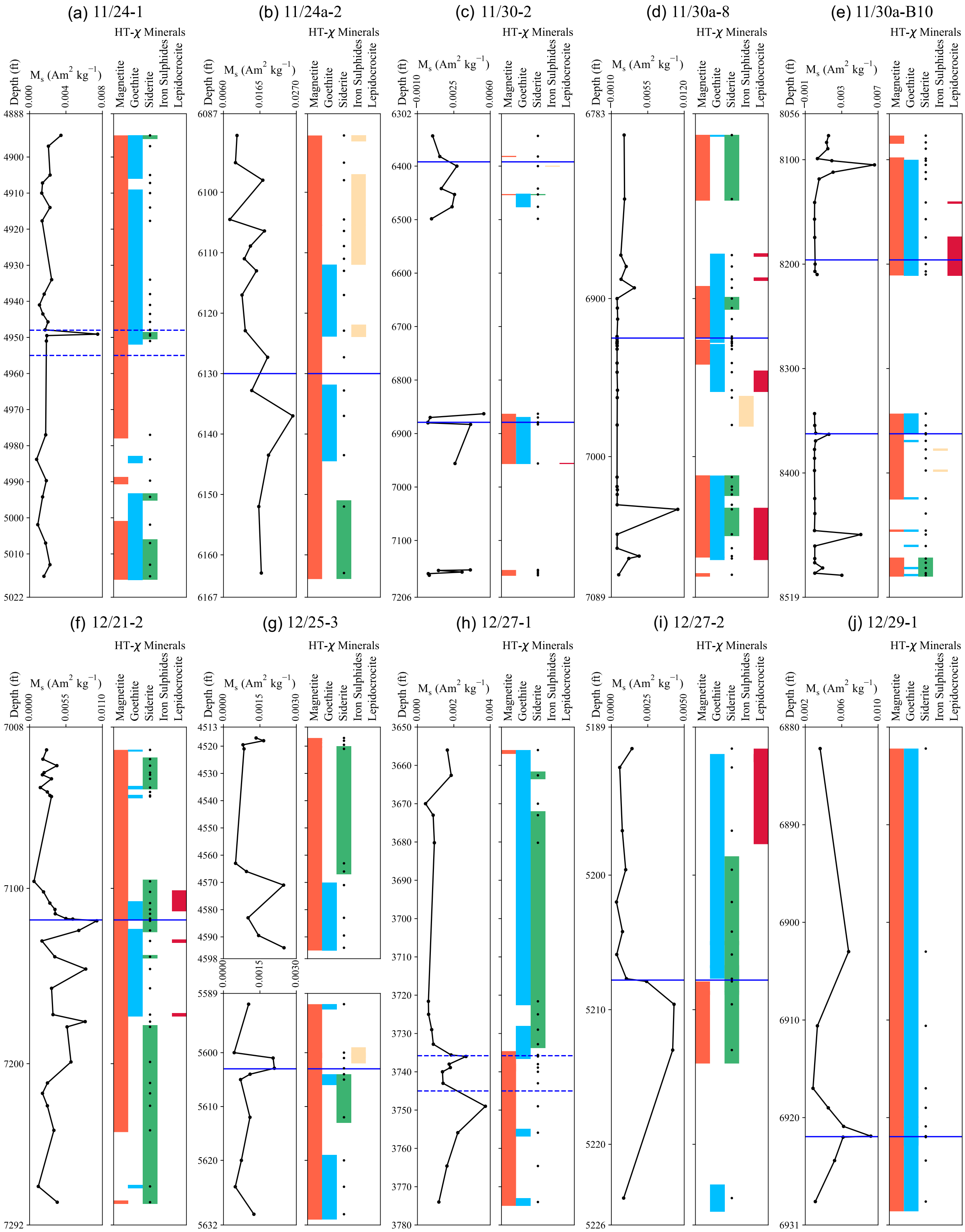

Figure 4. Room-temperature M_s versus depth in the vicinity of highlighted OWCs for 10 wells, plus a summary of the minerals identified through high-temperature susceptibility data for wells: 11/24-1 (a), 11/24a-2 (b), 11/30-2 (c), 11/30a-8 (d), 11/30a-B10 (e), 12/21-2 (f), 12/25-3 (g), 12/27-1 (h), 12/27-2 (i) and 12/29-1 (j). Note that the depth for each well is not consistent, and that therefore the y-axis scales vary between the wells. Black dots indicate sample points, blue lines indicate the locations of the OWCs in each well, with dashed blue lines indicating the location of OWC zones. Note the variable x-axis values within each sub-plot.

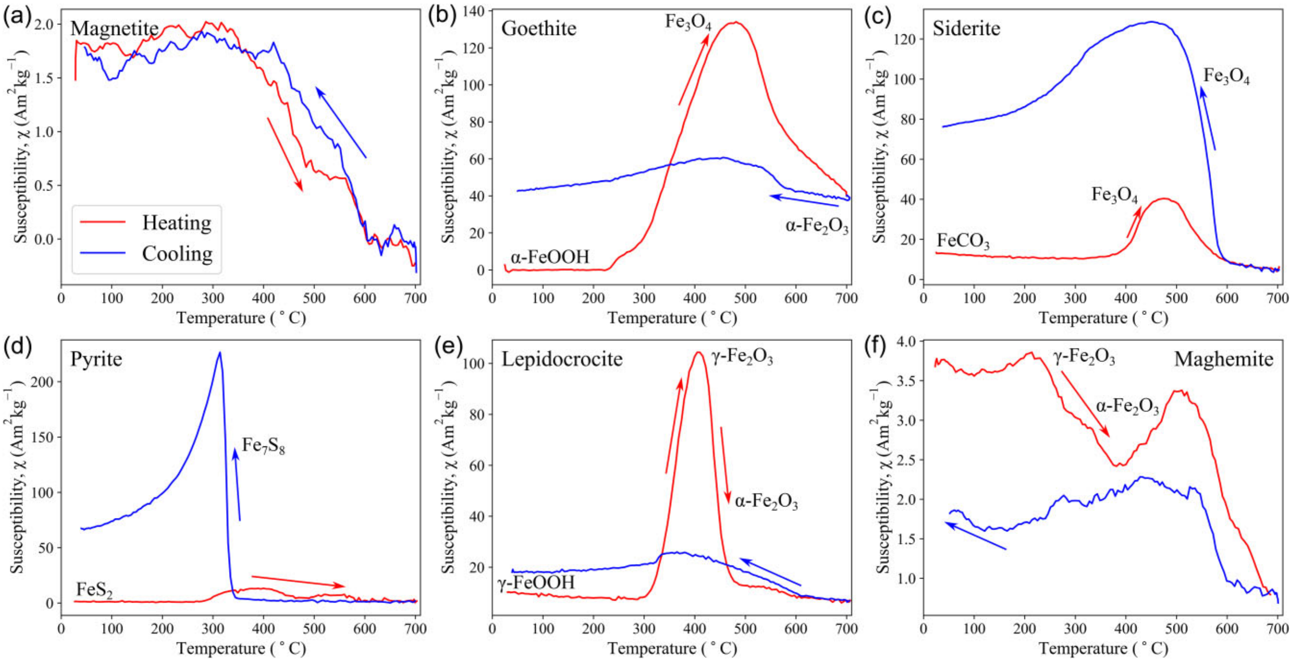

Figure 5. Example high-temperature susceptibility curves displaying a range of responses for the six individual magnetic minerals identified in this study: (a) magnetite (from 4517.0 ft, Well 12/25-3); (b) goethite (from 6925.5 ft, Well 11/30a-8); (c) siderite (from 5123.0 ft, Well 12/27-2); (d) pyrite (including formation of pyrrhotite; from 5600.0 ft, Well 12/25-3); (e) lepidocrocite (from 5190.6 ft, Well 12/27-2); (f) and maghemite (from 3738.9 ft, Well 12/27-1).

4.3 Scanning electron microscopy analysis

SEM and EDX analysis was carried out on samples from Well 11/30a-8: three samples in the oil-saturated sediments at 6900, 6906 and 6913 ft, and three samples in the water-saturated sediments at 7019, 7021 and 7024 ft, with these latter three being the same samples that underwent Mössbauer spectroscopy. The samples from the oil- and water-saturated sediments were found to be broadly similar, consisting of large siliceous, sandstone grains which were host to a wide variety of secondary minerals, including iron-rich minerals (Fig. 8). Within the images, several common iron-rich grains were: (1) $<1\ \mu$ m rod-like grains; (2) $<1\ \mu$ m globule-like grains and (3) larger ($>10\ \mu$ m) hexagonal plates (Figs 8a and c). It was not always possible to distinguish the mineralogy from EDX analysis, that is iron oxide, iron hydroxide or iron carbonate, as the samples were carbon coated. However, it is likely that rod-like grains and hexagonal plates were goethite given the morphologies (Hansel *et al.* 2003). Additionally, there were several occurrences of larger ($>5\ \mu$m) framboids formed of an amalgamation of partially octahedral grains (Fig. 8b); EDX indicated that these were iron oxides, suggesting magnetite. There was no evidence for iron sulphides in the samples.

5 DISCUSSION

An extensive data set was used in this study to analyse the magnetic mineral assemblages and behaviours across the IMF. Over 300 samples from various geological formation across the approximate 100 km^2 region were collected from drilled wells and analysed at room, high, and low temperatures to identify both magnetic mineral presence and characteristics. Iron oxides, hydroxides, carbonates, and sulphides were identified across the study region (Table 1).

We summarize the mineral magnetic signature using a pie charts to illustrate relative prevalence and distribution (Fig. 9); magnetite is excluded due to its ubiquity. These relative abundances, produced as ratios of number of samples containing the interpreted mineral to the total sample count in each well, are based on magnetizations of minerals to create a presence or absence identification, not volume/weight. This semi-quantitative relative abundance approach follows on from previous similar publications (e.g. Geiss & Zanner 2006; Yamazaki 2008; Abrajevitch *et al.* 2009) and is necessary because quantifying the absolute values of the different magnetic minerals is challenging. This is due to their relatively low concentrations, mixed minerals assemblages, the system not being magnetically closed and the qualitative nature of some of the identification methods used, for example high-temperature susceptibility. Given the relative spontaneous magnetizations of these magnetic minerals (Dunlop & Özdemir 1997), the absolute abundances may be very different to their relative abundances.

Goethite is the second most present magnetic mineral (after magnetite), being present in all the wells analysed. Following goethite, siderite is the next most abundant being present in nine of the twelve wells analysed. It is mainly present within water-saturated samples of the central and northern regions of the basin. Lepidocrocite is seen in the central wells of the basin, in all wells in the Beatrice Field, plus those in, and adjacent to, Jacky Field (Wells 11/30-2, 11/30-5, 11/30a-8, 11/30a-B10, 12/21-2, 12/21-4 and 12/27-2). Only one well shows evidence of maghemite, Well 12/27-1, creating a clear departure from the other wells in the basin. Iron sulphides, identified as pyrite altering to pyrrhotite at high temperatures, are seen most clearly within Well 11/24a-2 in the northern region of the basin. Iron sulphides are also seen in lower abundance within Well 12/25-3 in the eastern reaches of the basin, and very minorly in two wells in Beatrice Field (11/30a-8 and 11/30a-B10).

Connecting the presence of iron sulphides (Fig. 9) to the room-temperature magnetic properties (Table 1) produces a clear correlation—the extensive presence of iron sulphides in Well 11/24a-2 gives rise to the higher magnetizations in this well. These

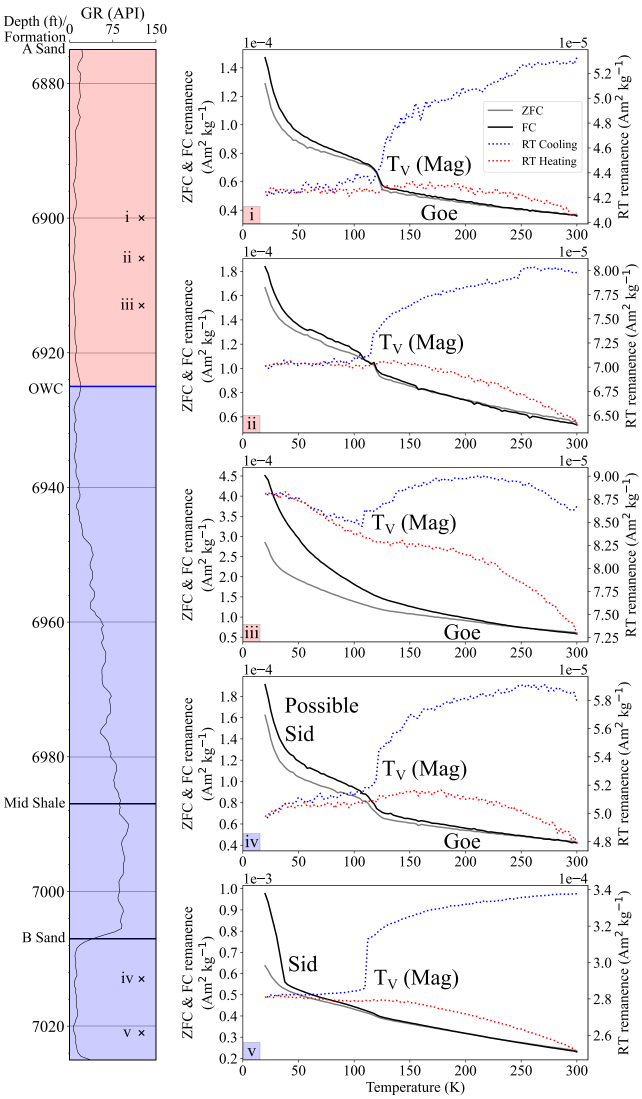

Figure 6. Examples of low-temperature magnetic data (FC, ZFC, SIRM) across the OWC of Well 11/30a-8 from the Beatrice Field, alongside a gamma ray (GR) well log plot showing the lithologies within which the samples were collected (a) sand for samples i–iii, (b) sand for samples iv–v. Magnetic phases identified are highlighted: (1) the Verwey transition (T_V) of magnetite, (2) typical ZFC and FC behaviour of siderite Housen (1996) and (3) goethite as described in the literature Liu *et al.* (2006).

findings are in contrast to previous studies of petroleum systems in the central North Sea (Badejo *et al.* 2021a, b; Abdulkarim *et al.* 2022a, b) which found iron sulphides to be abundant and goethite only in limited quantities.

5.1 Magnetic mineral assemblages in saturating fluids

The relative abundance of minerals in the two saturating fluids (oil and water) varies across the basin. The depth of oil-water contacts fluctuates across the IMF, occurring between 3735.8 ft (Well 1227-1) and 7118 ft (Well 12/21-2). There is no clear correlation identified between depth and magnetic mineral assemblage(s) (Fig. 4).

Goethite is the dominant mineral in eight out of ten oil-saturated sections, with the exceptions of Wells 11/24a-2 and 12/21-2 (Fig. 9). Comparatively, siderite is a minor presence in the oil-saturated sections of five wells, and the dominant magnetic mineral in another (Well 12/21-2). The only oil-saturated section not to be dominated by one of goethite or siderite is Well 11/24a-2, which contains a very high proportion of iron sulphides, mostly pyrite but with an accompanying ferrimagnetic phase, that is pyrrhotite or greigite.

In the water-saturated sections, the Beatrice Field wells have goethite-dominated water-saturated samples; in the wells to the immediate east of Beatrice, there is a higher proportion of siderite in the water-saturated sections than in the related oil-saturated sections. This siderite prevalence in water-saturated sections is most clearly seen in Wells 12/21-2 and 12/27-2, but also more subtly to the west, in Wells 11/24-1, 11/24a-2 and 12/25-3. In contrast, Wells 11/30-2, 11/30a-8, 11/30a-B10 and 12/27-1 show limited siderite presence in water-bearing sections of the wells (Table 1).

We have identified two clear trends in magnetization at OWCs (Table 2): one set of wells experience magnetic enhancement above the contact, for example Well 12/29-1, and another set of wells experience magnetic enhancement below the contact, for example Wells 11/24-1 and 12/27-1 (Fig. 4). Such enhancements have been reported previously (Badejo *et al.* 2021b); however, this study's findings are more nuanced, finding two different enhancements around the contacts.

Of the twelve wells in this study, ten contain OWCs, with two of the wells in Beatrice Field containing dual OWCs, resulting in 12 contacts (Figs 4 and 10; Table 2). Of these 12 contacts, three OWCs see increased magnetization above the contact, and seven have increased magnetization below the contact, plus there are two contacts, in Well 11/30a-8 and the upper OWC from Well 11/30a-B10, which show very subtle below-contact enhancement. The OWCs with enhanced magnetization above the contact come from wells 11/24a-2, 12/25-3 and 12/29-1, with the first and last of these being relatively better defined than 12/25-3. The OWCs with enhanced magnetization below the contact, that is in Wells 11/24-1, 11/30-2 (upper and lower), 11/30a-B10 (lower), 12/21-2, 12/27-1 and 12/27-2, are also of mixed clarity. Wells 11/24-1, 12/27-1 and 12/27-2 offer the best examples, whilst Well 11/30-2 is less conclusive due to the sampling constraints placed upon it, creating data gaps, alongside bearing two OWCs. The strongest example, Well 11/24-1 shows a clear, uninterrupted sharp increase in magnetization directly beneath the OWC, within the first 2 feet of the transitional OWC zone, which then proceeds to return back to baseline (Fig. 4).

The two types of enhancements show evidence of goethite and siderite with strong consistency (Figs 4 and 10). However, only the wells showing above-contact enhancement, Wells 11/24a-2 and 12/25-3, and wells with either unclear enhancement (11/30a-8) or more than one OWC (11/30-2 and 11/30a-B10) have clear presence of iron sulphides (Table 2; Fig. 4). In contrast, there is no definitive evidence of iron sulphides in any of the below-enhancement wells, bar the two OWC-bearing 11/30a-B10. The anomalous iron sulphide presence in Well 11/30a-B10 infers that a more complex redox environment, created by the layering of oil- and water-saturated lithologies, results in an unclassifiable well.

Furthermore, the wells that show no evidence of iron sulphides show an increased magnetic influence of magnetite and a decreasing influence of goethite towards the OWC. This behavioural pairing suggests that goethite is unstable around the contact and alters to magnetite. These enhancement characteristics and magnetic mineral behaviours form two broad classifications that divide the wells (Table 2; Fig. 10):

(i) Goethite-rich wells – these wells show no evidence of iron sulphides and often show magnetite-derived enhancement at the OWC, with a below-OWC enhancement.

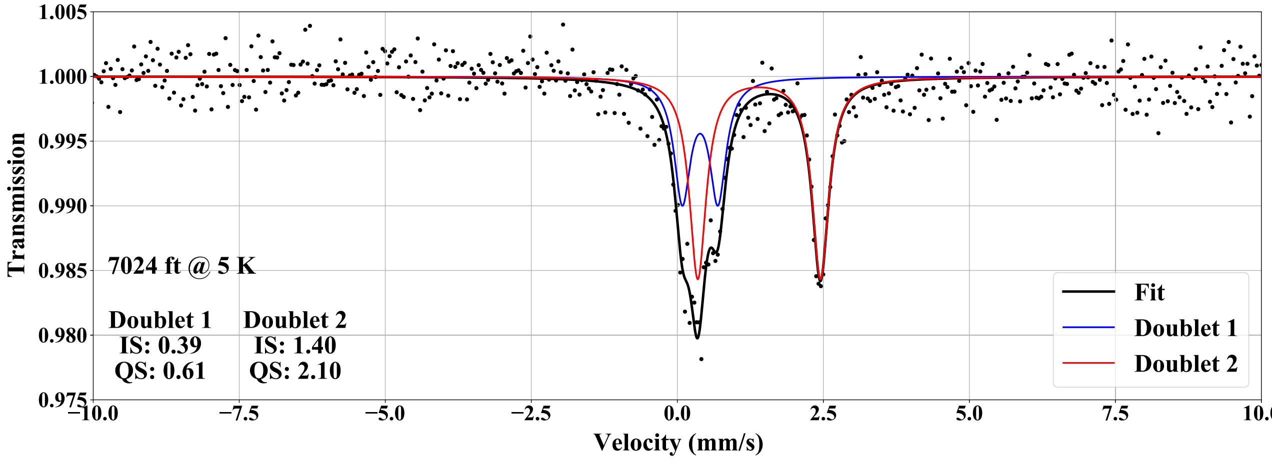

Figure 7. Low temperature (5 K) example Mössbauer spectra of a water-saturated sample at 7024 ft in Well 11/30a-8, showing an iron sulphide likely to be pyrite (Doublet 1) and ankerite (Doublet 2).

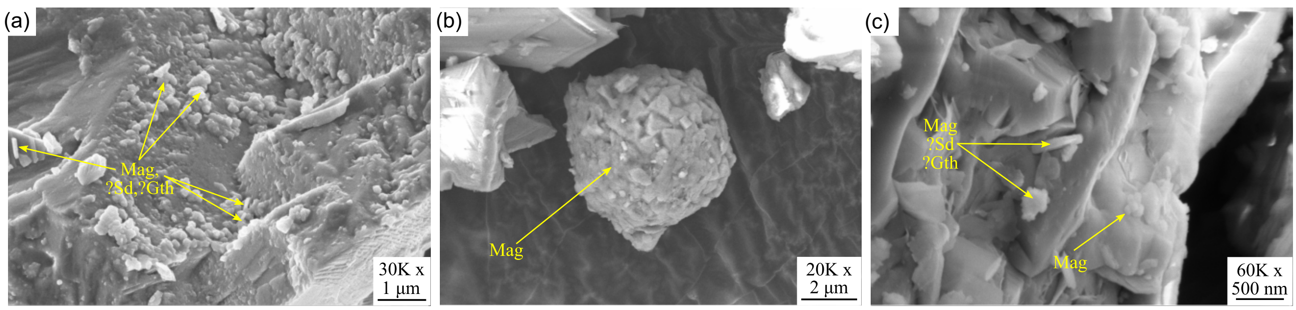

Figure 8. SEM images of water- and oil-saturated samples from Well 11/30a-8, showing magnetite, goethite and siderite presence. Gth, goethite; Mag, magnetite; Sd, siderite. Samples (a) and (b) are oil-saturated and (c) is water-saturated.

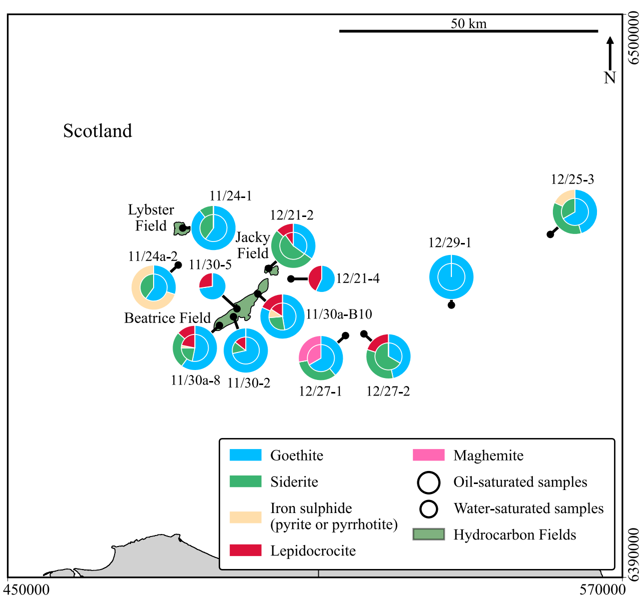

Figure 9. Mineral magnetic relative magnetic abundance across the IMF for the 12 studied wells depicted in pie charts. Magnetite is ignored as it is ubiquitous. The pie-charts are separated into oil- and water-saturated samples. Values are relative percentages of samples from each well and saturating fluid. These relative abundances are based on magnetizations not volume/weight. See Table 1 for sample totals. Note that the coordinate system is WGS 84 / UTM 30N.

(ii) Iron sulphide-rich wells – these wells show iron sulphide presence and are more goethite-poor, but still show presence of it and siderite, and have above-OWC enhancement.

Using this classification system, Wells 11/24-1, 12/21-2, 12/27-1 and 12/27-2 are goethite-rich wells; whereas Wells 11/24a-2 and 12/25-3 are iron sulphide-rich wells, with Wells 11/30-2, 11/30a-8, 11/30a-B10 and 12/29-1 being unclassified due to inconclusive OWC enhancement and the wells having two OWCs. The behaviour of the iron sulphide-rich wells in this study compare with the OWC-enhancement observed in iron sulphide-rich wells in the Central North Sea, sourced by the Kimmeridge Clay (Badejo *et al.* 2021a, b). Badejo *et al.* (2021b) identified above-contact enhancement alongside high levels of iron sulphide in the Type II-sourced system, which also lacked iron-sulphide-free/goethite-rich wells.

5.2 Origin of magnetic minerals

The iron hydroxides goethite and lepidocrocite are thought to have formed before the migration of oil, and are likely to be authigenic. This is because goethite and lepidocrocite indicate the presence of anaerobic sediments in lacustrine deposits (Fortin *et al.* 1993; Van der Zee *et al.* 2003) and in red beds (Berner 1969; Weibel 1999; Gendler *et al.* 2005), through the precipitation of magnetic minerals, and the alteration of detrital magnetite alongside iron from clay minerals, respectively. These environments were present during the deposition of the Devonian sediments within the IMF, offering a potential source of iron hydroxides directly within a hydrocarbon

Table 2. Table summarising the OWC locations and depths (in MD, bar 11/30a-B10 which is TVD), magnetic responses and magnetic minerals present the wells studied in the IMF, ignoring the pervasive magnetite, separated by saturating fluid and the classification of each OWC-bearing well, based on its characteristics. Fm, formation; goe, goethite; FeS, iron sulphides; lep, lepidocrocite; mgh, maghemite; sid, siderite.

Well	Field	OWC-bearing Fm, depth (ft)	Magnetic enhancement relative to OWC	HT-χ and LT identified minerals Oil	Water	Classification
11/24-1	Lybster	B Sand, 4948	Below	goe	goe, sid	Goe-rich
11/24a-2	–	A Sand, 6130	Above	FeS, goe	goe, sid	FeS-rich
11/30-2	Beatrice	A Sand, 6385	Below	goe	goe, sid, lep	Goe-rich
		H Sand, 6879	Below			
11/30a-8	Beatrice	A Sand, 6925	?Below	goe, sid, lep	goe, sid, lep, FeS	?
11/30a-B10	Beatrice	I Sand, 6643	?Below	goe, sid, lep	goe, sid, lep, FeS	?Goe-rich
		J Sand, 6753	Below			
12/21-2	Jacky	B Sand, 7118	Below	sid, goe, lep	sid, goe, lep	Goe-rich
12/25-3	–	Cr. Knoll, 5603	Above	goe, sid, FeS	goe, sid	FeS-rich
12/27-1	–	Pentland, 3735.8	Below	goe, sid, mgh	goe, mgh	Goe-rich
12/27-2	–	B Sand, 5207.8	Below	goe, sid, lep	sid, goe	Goe-rich
12/29-1	–	Heather, 6921.95	Above	goe	goe	?

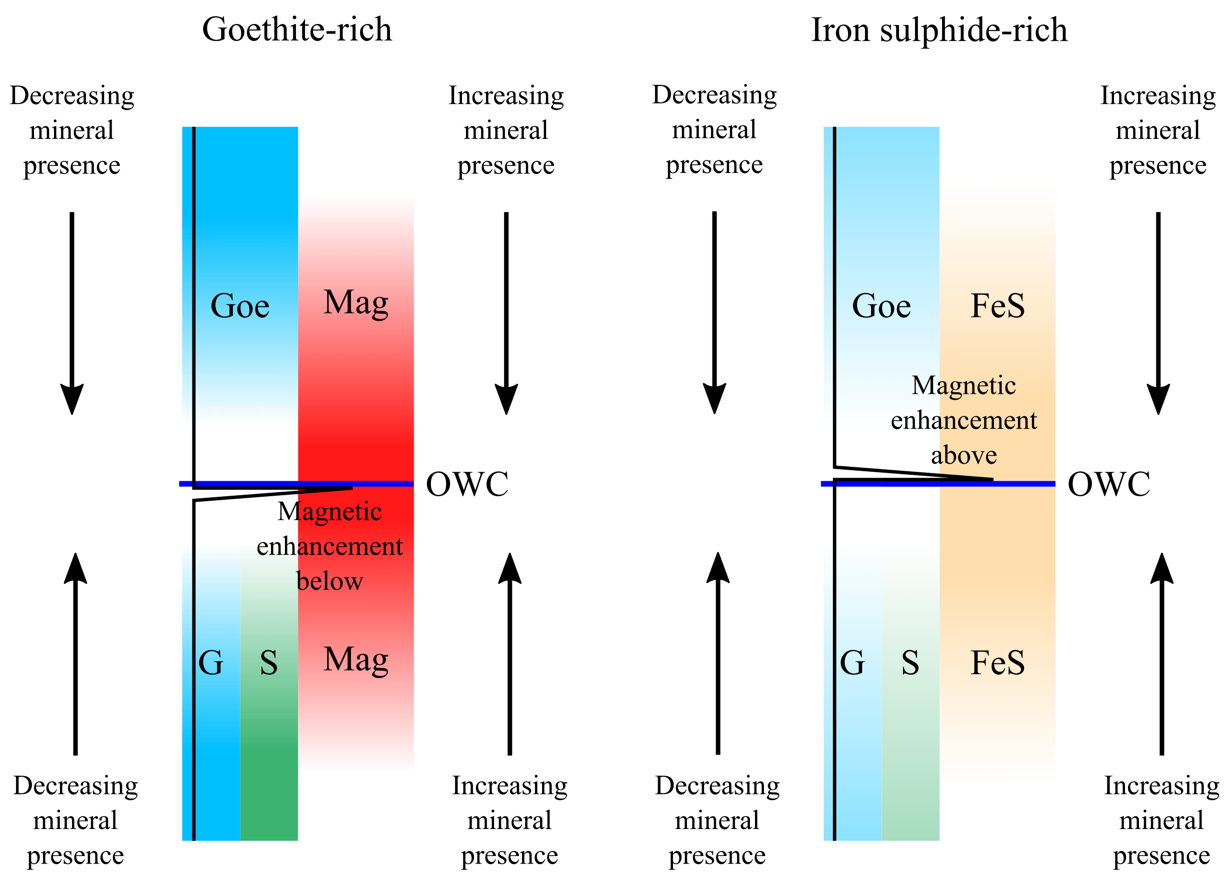

Figure 10. Schematic of two models showing how magnetic minerals interact around oil-water contacts in the IMF. Wells dominated by goethite (Goe, G) see decreasing goethite signals towards the OWC in tandem with increasing magnetite (Mag) presence towards the contact, with siderite (S) present in wells that experience extensive vertical migration of the hydrocarbons. Wells with low concentrations of goethite see this same pattern, but with increasing iron sulphide (FeS)-presence towards the OWC.

source rock. Lepidocrocite is metastable, and is often considered a pre-cursor to goethite on the reaction pathway; however, lepidocrocite can alter into maghemite through topotactic thermal dehydration and dehydroxylation (Cudennec & Lecerf 2005; Gendler *et al.* 2005; Guyodo *et al.* 2016; Song & Boily 2016; Cheng *et al.* 2019). This is likely, although not confirmed, the mechanism for the presence of maghemite in Well 12/27-1.

Magnetite is ubiquitous across the IMF. Given its relatively high spontaneous magnetization, only low concentrations of it are required to be identified. It is likely that some of the magnetite is detrital in origin, though there is strong evidence that additional magnetite forms near the OWC apparently at the expense of goethite (Figs 4 and 6). Small amounts of magnetite are thought to form as an interstitial phase along the dehydroxylation path of goethite to hematite (Cudennec & Lecerf 2005; Till & Nowaczyk 2018), though other mechanisms have been suggested (Lima-de-Faria 1967; Lowrie & Heller 1982; Goss 1987; Ibrahim *et al.* 1994). For example, goethite can alter to magnetite in the presence of organic matter (Schwertmann & Fechter 1984), as well as through reductive diagenetic alteration (Rude & Aller 1989; Abrajevitch *et al.* 2009). It is clear that, due to the increase in magnetization and identification of magnetite, we interpret that magnetite forms at the OWC, but it may also form from goethite within the water-saturated sediments during hydrocarbon migration. Hydrocarbons provide the required organic matter for alteration, with the newly formed magnetite being transported with the migrating hydrocarbons (Badejo *et al.* 2021b), before accumulating at the fluid density boundary. As magnetite forms and remains stable in a variety of conditions, the ubiquitous nature of the mineral makes constraining its significance on the IMF difficult.

The formation of siderite requires dissolved Fe^{2+} iron and carbonate ions ($CO_3{}^2$) to react within anoxic conditions in the absence of hydrogen sulphides (Berner 1981; Lin *et al.* 2020). As such, the reducing environments created by hydrocarbons provide ideal conditions to allow siderite to form (Machel & Burton 1991; Machel 1995; Emmerton *et al.* 2013). Abdulkarim *et al.* (2022a) suggests that during upward vertical migration of hydrocarbons, due to the reduction in pressure there is a release of both carbon and oxygen which leads to the formation of siderite, that is the presence of siderite is evidence for upward vertical migration of hydrocarbons. Given the abundance of siderite in the IMF, we infer that all of the known hydrocarbon accumulations within the IMF, that is Beatrice, Lybster and Jacky Fields, could be charged, to some degree, by vertical migration; the wells in the three fields, that is Wells 11/24-1, 11/30-2, 11/30a-8, 11/30a-B10 and 12/21-2, all show evidence of siderite.

Iron sulphides, predominantly pyrite, form and are stable, in reducing environments, such as those formed by hydrocarbon accumulations (Machel & Burton 1991; Machel 1995). Consequently, the magnetic enhancement seen in iron sulphide-rich wells being situated above the OWC is likely a result of accumulation and formation of stable minerals above the OWC in the oil column. Iron sulphides are found within the north west IMF (Table 1); however, generally iron sulphides are far less common than elsewhere in the North Sea (Badejo *et al.* 2021a; Abdulkarim *et al.* 2022b). This study only identified pyrite and pyrrhotite, but no greigite unlike some Central North Sea studies (Badejo *et al.* 2021a). Geochemical analyses of the IMF hydrocarbons (Peters *et al.* 1989) suggest that the Devonian and Pentland hydrocarbons have low sulphur content (maximum 0.62 wt per cent), as does the mixed oil itself (0.11 wt per cent). In contrast, Kimmeridge Clay black shales have a much higher sulphur content of 2.59 wt per cent (Peters *et al.* 1989). This variance suggests that the Devonian and Pentland source rocks are not sulphur contributors, but that the Kimmeridgian black shales is. The Central North Sea is predominantly charged by the Kimmeridgian black shales (Badejo *et al.* 2021a; Abdulkarim *et al.* 2022b). Therefore, it is likely that hydrocarbon charging in the north west IMF is of a Kimmeridgian black shales origin.

It should be noted that iron sulphides can also be formed by bacteria during biodegradation (Emmerton *et al.* 2013; Thiel *et al.* 2019; Badejo *et al.* 2021a); however, the geochemical analysis of Peters *et al.* (1989) suggests biodegradation is limited in the IMF as most of the hydrocarbon reservoirs are too deep. Despite this, some samples and wells are shallow enough and encounter sufficiently low temperatures (∼40 °C), to potentially experience biodegradation, although, there is no indication that biodegradation has influenced the iron sulphide-bearing samples and wells. However, biodegradation analysis and geothermal modelling are beyond the scope of this study, thus cannot be ruled out with complete certainty.

5.3 Combining magnetic mineralogical and petroleum system information

Here we compare the magnetic mineralogical signals in the IMF to the BPSM results of Perkins (2022) and Perkins *et al.* (2023). We consider the relative abundance of five minerals: goethite, siderite, lepidocrocite, maghemite and iron sulphides to represent the magnetic mineral behaviour and compare them to mixing ratios from the three hydrocarbon sources, that is the Devonian Fish Beds, the Pentland Formation and the Kimmeridge Clay, determined from BPSM (Table 3). Goethite is present in all the wells, in both saturating fluids, matching the mixing ratios that show presence, in all wells, of Devonian and Pentland hydrocarbon contributions (Table 3). In contrast, there are no correlations between mixing ratios and siderite presence, indicating that siderite within the magnetic mineral assemblage is likely a result of vertical migration, not differing hydrocarbon sources. Lepidocrocite and maghemite are only identified within Type I- and II-III-sourced wells, with the connections between goethite, lepidocrocite and maghemite to Type I and II–III depositional environments offering potential indicator minerals for these kerogen types. In contrast, the correlation between Type II source rocks and iron sulphides, as seen in Well 11/24a-2, presents these iron sulphides as potential indicator minerals for Type II kerogen-bearing source rocks (Table 3).

Well 11/24a-2 shows the only >50 per cent Kimmeridge Clay black shales hydrocarbon contribution alongside a dominant iron sulphide presence, with a much lower percentage of Devonian and Pentland indicator minerals. The preferential formation of iron sulphides in sulphur-rich environments likely inhibited the presence of other magnetic minerals. The connection between iron-sulphide presence/absence and hydrocarbon source type as seen in Well 11/24a-2 is supported by the iron sulphide-rich, Type II Kimmeridge Clay-charged petroleum systems of the Central North Sea studied by Abdulkarim *et al.* (2022a, b) and Badejo *et al.* (2021a, b).

Of the wells with no iron sulphide presence, only Well 12/21-2, in Jacky Field, has <75 percent of samples containing at least one of goethite, lepidocrocite or maghemite (Table 3). The cause of this is unclear; however, it is the only well dominated by siderite, with 24 of 33 samples (73 percent) showing evidence of the iron carbonate (Fig. 9). Consequently, it could be hypothesized that siderite has either preferentially formed, or migrated into, the Well 12/21-2 region, a process supported by research in the central North Sea from Abdulkarim *et al.* (2022a).

6 CONCLUSION

Magnetic mineral assemblages across the IMF show broad trends that are magnified at well-scale, in particular associated with the OWCs (Fig. 10). In the wells that contain OWCs, clear magnetic enhancements are seen at OWCs in eight of the ten wells (Fig. 4), in agreement with previous studies (Badejo *et al.* 2021b; Abdulkarim *et al.* 2022c). We show for the first time, that some wells experience magnetic enhancement above the contact, and others experience it below. These enhancement trends correlate to magnetic minerals identified within the wells, allowing for classification of the wells into two groups: (1) the goethite-rich group and (2) the iron-sulphide-rich group (Fig. 10).

Table 3. Mixing ratios of the Devonian Fish Beds (Dev.), Pentland Formation source rocks (Pent.), and the Kimmeridge Clay source rocks (Kimm. Clay) with the IMF, with kerogen types shown in brackets, and the relative abundance of goethite (goe.), siderite (sid.), lepidocrocite (lep.), maghemite (mgh.) and iron sulphides (FeS) in the oil-saturated samples within the reservoir units of the IMF. The mixing ratios are calculated using BPSM models of Perkins (2022) and Perkins *et al.* (2023). The relative abundance of minerals is used, that is how often a magnetic mineral was detected, rather than the absolute, as direct abundance estimates are not possible. Note that multiple minerals can occur concurrently within samples, but this does not impact the count.

Well	Field	Source contribution (per cent)			Sum of Devonian and Pentland (per cent)	Total number of samples	Relative mineral abundance (per cent)				
		Dev. (I)	Pent. (II-III)	Kimm. Clay (II)			goe.	sid.	lep.	mgh.	FeS
11/24-1	Lybster	59	40	1	99	16	94	13	0	0	0
11/24a-2	–	0	49	51	49	11	27	0	0	0	64
11/30-2	Beatrice	57	43	0	100	5	60	0	0	0	0
11/30a-8	Beatrice	40	60	0	100	10	90	40	20	0	0
11/30a-B10	Beatrice	100	0	0	100	12	77	0	15	0	0
12/21-2	Jacky	71	29	0	100	17	47	76	18	0	0
12/27-1	–	78	22	0	100	15	60	47	0	33	0
12/27-2	–	54	46	0	100	8	88	63	38	0	0
12/29-1	–	57	43	0	100	7	86	0	0	14	0

The goethite-rich group is the most dominant, comprising six of the ten OWC-bearing wells. The goethite-rich wells contain no iron sulphides, but strong presence of goethite and siderite, accompanied by below-OWC magnetic enhancements. The iron sulphide-rich group is represented by two OWC-bearing wells. The iron sulphide-rich wells show less goethite, in tandem with a clear iron sulphide presence, and an above-OWC magnetic enhancement. In addition, the goethite-rich wells show increasing ferrimagnetic material around the OWCs, in the form of magnetite. This increase in ferrimagnetic component is thought to be connected to the alteration of unstable goethite into magnetite at the contact, caused by the variable redox conditions.

Siderite presence is connected to vertical hydrocarbon migration instead of forming through a different process, in alignment with other regions of the North Sea (Badejo *et al.* 2021a; Abdulkarim *et al.* 2022a). Presence of goethite and lepidocrocite is indicative of a non-Type II petroleum system (Peters *et al.* 2004). Type II systems are typically more iron sulphide-dominant, inferring a connection between the formation of iron hydroxides and Type I and II–III source rocks, which have both been proven to generate hydrocarbons in the IMF (Perkins *et al.* 2023). This connection is further amplified by the formation of iron hydroxides within lacustrine and lagoonal-to-shallow marine environments (Berner 1969; Gendler *et al.* 2005), both of which occur in the IMF through the Devonian and Pentland Formation source rocks, respectively.

This study affirms a connection between iron sulphides and Type II kerogen, produced within deep marine-deposited source rocks (Badejo *et al.* 2021a; Abdulkarim *et al.* 2022a). Well 11/24a-2 in the IMF is shown to have a Type II-dominated hydrocarbon mix, primarily sourced by the Kimmeridge Clay black shales, and is the only well in the IMF that has a high proportional presence of iron sulphides in oil-saturated samples in the basin (Perkins *et al.* 2023).

This study has shown how the IMF is characterized by a variable magnetic mineral assemblage that can be directly linked to its petroleum system (Perkins *et al.* 2023). This connection, predominantly between magnetic minerals and source rock kerogen type, expand beyond previous relationships between magnetic minerals and hydrocarbons. The identification of: (1) two clear and separate magnetic mineral assemblages based on source rock kerogen type; (2) differing magnetic mineral enhancements based on these magnetic mineral assemblages and (3) the interweaving of magnetic mineral presence as a proxy for migration methods, shows, for the first time, the opportunity to loosely define a petroleum system solely from its magnetic mineral assemblages. In turn, the connections delineated in this study provide a new method to corroborate conventional analytical techniques for defining petroleum systems (e.g. geophysical logging, geochemistry and petroleum system modelling).

DATA AVAILABILITY

All data presented here is available both within the PhD thesis of Perkins (2022) (doi:10.25560/101317), or data can be accessed directly from Zenodo.org (doi:10.5281/zenodo.10835519; Perkins, 2024).

ACKNOWLEDGMENTS

J.R.P. would like to thank the Engineering and Physical Sciences Research Council (EPSRC) for funding this research through its doctoral studentship grant (EP/R513052/1); the British Geological Survey for access to core samples and the I.R.M. at the University of Minnesota, Minneapolis, for granting two Visiting Fellowships.

REFERENCES

Abdulkarim, M.A., Muxworthy, A.R. & Fraser, A.J., 2022c. High-temperature susceptibility (HT-χ) measurements: A potential tool for the identification of oil water transition zone (OWTZ) in petroleum reservoirs, *Front. Earth Sci.,* **10,** doi:10.3389/feart.2022.973385.

Abdulkarim, M.A., Muxworthy, A.R., Fraser, A.J., Neumaier, M., Hu, P. & Cowan, A., 2022a. Siderite occurrence in petroleum systems and its potential as a hydrocarbon-migration proxy: a case study of the catcher area development and the Bittern area, UK North Sea, *J. Petrol. Sci. Eng.,* **212,** 1–15.

Abdulkarim, M.A., Muxworthy, A.R., Fraser, A.J., Sims, M. & Cowan, A., 2022b. Effect of hydrocarbon presence and properties on the magnetic signature of the reservoir sediments of the catcher area development region, UK North Sea, *Front. Earth Sci.,* **10,** 1–20.

Abrajevitch, A., Van der Voo, R. & Rea, D.K., 2009. Variations in relative abundances of goethite and hematite in Bengal Fan sediments: Climatic vs. diagenetic signals, *Mar. Geol.,* **267**(3–4), 191–206.

Abubakar, R., Muxworthy, A.R., Fraser, A.J., Sephton, M.A., Watson, J.S., Heslop, D., Paterson, G.A. & Southern, P., 2020. Mapping hydrocarbon charge-points in the Wessex Basin using seismic, geochemistry and mineral magnetics, *Mar. Petrol. Geol.,* **111,** 510–528.

Abubakar, R., Muxworthy, A.R., Sephton, M.A., Southern, P., Watson, J.S., Fraser, A.J. & Almeida, T.P., 2015. Formation of magnetic minerals at hydrocarbon-generation conditions, *Mar. Petrol. Geol.,* **68,** 509–519.

Andrews, I.J., Long, D., Richards, P.C., Thomson, A.R., Brown, S., Chesher, J.A. & McCormac, M., 1990. *The Geology of the Moray Firth, United Kingdom Offshore Regional Report,* British Geological Survey, Keyworth, Nottingham.

Badejo, S.A., Muxworthy, A.R., Fraser, A.J., Neumaier, M., Perkins, J.R., Stevenson, G.R. & Davey, R., 2021a. Using magnetic techniques to calibrate hydrocarbon migration in petroleum systems modelling: A case study from the Lower Tertiary, UK Central North Sea, *Geophys. J. Int.,* **227**(1), 617–631.

Badejo, S.A., Muxworthy, A.R., Fraser, A.J., Stevenson, G.R., Zhao, X. & Jackson, M., 2021b. Identification of magnetic enhancement at hydrocarbon-fluid contacts, *AAPG Bull.,* **105**(10), 1973–1991.

Berner, R.A., 1969. Goethite stability and the origin of red beds, *Geochim. Cosmochim. Acta,* **33**(2), 267–273.

Berner, R.A., 1981. A new geochemical classification of sedimentary environments, *SEPM J. Sediment. Res.,* **51**(2), 359–366.

Besnus, M.J. & Meyer, A.J., 1964. 'Nouvelles donnees experimentales sur le magnetisme de la pyrrhotine naturelle', in *Proceedings of the International Conference on Magnetism,* Nottingham, September 1964, pp. 507–511.

Brown, S., Richards, P.C., Andrews, I.J. & Thomson, J.R., 1988. *Stratigraphic Evolution and Reservoir Sedimentology, Moray Firth Basin: A Core workshop,* Hydrocarbons Research Programme report, British Geological Survey, Edinburgh.

Cheng, Y., Xing, J., Bu, C., Zhang, J., Piao, G., Huang, Y., Xie, H. & Wang, X., 2019. Dehydroxylation and structural distortion of kaolinite as a high-temperature sorbent in the furnace, *Minerals,* **9**(10), 587–603.

Cudennec, Y. & Lecerf, A., 2005. Topotactic transformations of goethite and lepidocrocite into hematite and maghemite, *Solid State Sci.,* **7**(5), 520–529.

Day, R., Fuller, M. & Schmidt, V.A., 1977. Hysteresis properties of titanomagnetites: Grain-size and compositional dependence, *Phys. Earth planet. Inter.,* **13**(4), 260–267.

Dunlop, D.J. & Özdemir, Ö., 1997. *Rock Magnetism: Fundamentals and Frontiers,* Cambridge Univ. Press.

Dunlop, D.J., 2002. Theory and application of the Day plot (M_{rs}/M_s versus H_{cr}/H_c) 1. Theoretical curves and tests using titanomagnetite data, *J. geophys. Res.,* **107**(B3), doi:10.1029/2001JB000486.

Elmore, R.D. & Crawford, L., 1990. Remanence in authigenic magnetite: testing the hydrocarbon-magnetite hypothesis, *J. geophys. Res.,* **95**(B4), 4539–4549.

Elmore, R.D., Engel, M.H., Crawford, L., Nick, K., Imbus, S. & Sofert, Z., 1987. Evidence for a relationship between hydrocarbons and authigenic magnetite, *Nature,* **325**(29), 428–430.

Elmore, R.D., Muxworthy, A.R. & Aldana, M., 2012. Remagnetization and chemical alteration of sedimentary rocks, *Geol. Soc. Spec. Publ.,* **371**(1), 1–21, doi:10.1144/SP371.15.

Emmerton, S.A., Muxworthy, A.R., Sephton, M.A., Aldana, M., Costanzo-Álvarez, V., Bayona, G. & Williams, W., 2013. Correlating biodegradation to magnetization in oil bearing sedimentary rocks, *Geochim. Cosmochim. Acta,* **112,** 146–165.

Evans, B.J., Johnson, R.G., Senftle, F.E., Cecil, C.B. & Dulong, F., 1982. The ^{57}Fe Mössbauer parameters of pyrite and marcasite with different provenances, *Geochim. Cosmochim. Acta,* **46**(5), 761–775.

Fortin, D., Leppard, G.G. & Tessier, A., 1993. Characteristics of lacustrine diagenetic iron oxyhydroxides, *Geochim. Cosmochim. Acta,* **57**(18), 4391–4404.

Geiss, C.E. & Zanner, C.W., 2006. How abundant is pedogenic magnetite? Abundance and grain size estimates for loessic soils based on rock magnetic analyses, *J. geophys. Res.,* **111**(B12S21), doi:10.1029/2006JB004564.

Gendler, T.S., Shcherbakov, V.P., Dekkers, M.J., Gapeev, A.K., Gribov, S.K. & McClelland, E., 2005. The lepidocrocite-maghemite-haematite reaction chain - I. Acquisition of chemical remanent magnetization by maghemite, its magnetic properties and thermal stability, *Geophys. J. Int.,* **160**(3), 815–832.

Glennie, K., Higham, J. & Stemmerik, L., 2003. Chapter 8 - Permian, in *The Millenium Atlas: Petroleum Geology of the Central and Northern North Sea,* pp. 91–103, eds Evans, D., Graham, C., Armour, A. & Bathurst, P., Geological Society of London.

Goss, C.J., 1987. The kinetics and reaction mechanism of the goethite to hematite transformation, *Mineral. Mag.,* **51,** 437–451.

Greenhalgh, E.E., 2016. *Literature Review of Devonian Source Rocks and Devonian-Sourced Hydrocarbons in the Orcadian Basin,* Energy and Marine Geoscience Programme Commissioned Report CR/16/017, British Geological Survey, Keyworth, Nottingham.

Guyodo, Y., Bonville, P., Till, J.L., Ona-Nguema, G., Lagroix, F. & Menguy, N., 2016. Constraining the origins of the magnetism of lepidocrocite (γ-FeOOH): a Mössbauer and magnetization study, *Front. Earth Sci.,* **4,** 1–9.

Hansel, C.M., Benner, S.G., Neiss, J., Dohnalkova, A., Kukkadapu, R.K. & Fendorf, S., 2003. Secondary mineralization pathways induced by dissimilatory iron reduction of ferrihydrite under advective flow, *Geochim. Cosmochim. Acta,* **67**(16), 2977–2992.

Harker, S.D. & Rieuf, M., 1996. Genetic stratigraphy and sandstone distribution of the Moray Firth Humber Group (Upper Jurassic), *Geol. Soc., Lond., Spec. Publ.,* **114,** 109–130.

Hillis, R.R., Thomson, K. & Underhill, J.R., 1994. Quantification of tertiary erosion in the inner moray firth using sonic velocity data from the chalk and the kimmeridge clay, *Mar. Petrol. Geol.,* **11**(3), 283–293.

Hilscher, G., Rogl, P., Zemann, J. & Ntaflos, T., 2005. Low-temperature magnetic investigation of ankerite, *Eur. J. Mineral.,* **17**(1), 103–105.

Housen, B.A., Banerjee, S.K. & Moskowitz, B.M., 1996. Low-temperature magnetic properties of siderite and magnetite in marine sediments, *Geophys. Res. Lett.,* **23**(20), 2843–2846.

Ibrahim, M.M., Edwards, G., Seehra, M.S., Ganguly, B. & Huffman, G.P., 1994. Magnetism and spin dynamics of nanoscale FeOOH particles, *J. Appl. Phys.,* **75**(10), 5873–5875.

J.R., Perkins 2024. *Supporting database to publication*. doi.org/10.1093/gji/ggae254.

Kantorowicz, J.D., 1985. The origin of authigenic ankerite from the Ninian Field, UK North Sea, *Nature,* **315,** 214–216.

Kar, S., Mandal, S.K., Das, D. & Chaudhuri, S., 2004. Wet chemical synthesis of iron pyrite and characterisation by Mössbauer spectroscopy, *Mater. Lett.,* **58**(22–23), 2886–2889.

Lima-de-Faria, J., 1967. Anomalous orientations of cubic close packing in the dehydration of Goethite in an inert atmosphere, *Acta Crystallograph.,* **23,** 733–736.

Lin, C.Y., Turchyn, A.V., Krylov, A. & Antler, G., 2020. The microbially driven formation of siderite in salt marsh sediments, *Geobiology,* **18**(2), 207–224.

Linsley, P.N., Potter, H.C., McNab, G. & Racher, D., 1980. The Beatrice Field, Inner Moray Firth, UK., North Sea, in *Giant Oil and Gas Fields of the Decade 1968-1978,* pp. 117–129, ed. Halbouty, M.T., American Association of Petroleum Geologists.

Liu, Q., Yu, Y., Torrent, J., Roberts, A.P., Pan, Y. & Zhu, R., 2006. Characteristic low-temperature magnetic properties of aluminous goethite [$alpha$-(Fe,Al)OOH] explained, *J. geophys. Res.,* **111**(B12), doi:10.1029/2006JB004560.

Lowrie, W. & Heller, F., 1982. Magnetic properties of marine limestones, *Rev. Geophys.,* **20**(2), 171–192.

Machel, H.G. & Burton, E.A., 1991. Chemical and microbial processes causing anomalous magnetization in environments affected by hydrocarbon seepage, *Geophysics,* **56**(5), 598–605.

Machel, H.G., 1995. Magnetic mineral assemblages and magnetic contrasts in diagenetic environments - with implications for studies of palaeomagnetism, hydrocarbon migration and exploration, in *Palaeomagnetic Applications in Hydrocarbon Exploration and Production,* pp. 9–29, eds Turner, P. & Turner, A., Geological Society Special Publications.

Minyuk, P.S., Subbotnikova, T.V. & Plyashkevich, A.A., 2011. Measurements of thermal magnetic susceptibility of hematite and goethite, *Izvest., Phys. Solid Earth,* **47**(9), 762–774.

Minyuk, P.S., Tyukova, E.E., Subbotnikova, T.V., Kazansky, A.Y. & Fedotov, A.P., 2013. Thermal magnetic sysceptibility data on natural iron sulphides of northeastern Russia, *Russ. Geol. Geophys.,* **54**(4), 464–474.

Morin, F.J., 1950. Magnetic susceptibility of α-Fe_2O_3 and α-Fe_2O_3 with added titanium, *Phys. Rev.,* **78**(6), 819–810.

Muxworthy, A.R., Turney, J.N., Qi, L., Baker, E. B., Perkins, J.R. & Abdulkarim, M. A., 2023. Interpreting high-temperature magnetic susceptibility data of natural systems, *Front. Earth Sci.,* **11,** doi:10.3389/feart.2023.1171200.

Perkins, J.R., 2022. Hydrocarbon source and migration pathway identification through basin and petroleum systems modelling and mineral magnetism: a case study on the Beatrice Field, Inner Moray Firth, UK North Sea, *PhD thesis*, Imperial College London, UK.

Perkins, J.R., Fraser, A.J., Muxworthy, A.R., Neumaier, M. & Schenk, O., 2023. Utilising basin and petroleum systems modelling (BPSM) to characterise multi-source hydrocarbon generation, identify migration pathways and unravel hydrocarbon mixing ratios in a poorly-understood basin: a case study on the Inner Moray Firth, UK North Sea, *Mar. Petrol. Geol.,* **151,** doi:10.1016/j.marpetgeo.2023.106180.

Peters, K.E., Moldowan, J.M., Driscole, A.R. & Demaison, G.J., 1989. Origin of beatrice oil by co-sourcing from Devonian and middle Jurassic source rocks, inner moray firth, United Kingdom, *AAPG Bull.,* **73**(4), 454–471.

Peters, K.E., Walters, C.C. & Moldowan, J.M., 2004. *The Biomarker Guide,* 2nd edn, Cambridge Univ. Press.

Reeder, R.J. & Dollase, W.A., 1989. Structural variation in the dolomite-ankerite solid-solution series: and X-ray, Mössbauer, and TEM study, *Am. Mineral.,* **74,** 1159–1167.

Richards, R.P., Lott, G.K., Johnson, H., Knox, R.W.O'B. & Riding, J.B., 1993. 3. Jurassic of the central and northern North Sea, in *Lithostratigraphic Nomenclature of the UK North Sea,* pp. 252, eds Knox, R.W.O'B. & Cordey, W.G., British Geological Survey.

Ristic, M., Krehula, S., Reissner, M. & Music, S., 2017. ^{57}Fe Mössbauer, XRD, FT-IR, FE SEM analyses of natural goethite, hematite and siderite, *Croat. Chem. Acta,* **90**(3), 499–507.

Roberts, A.M., Badley, M.E., Price, J.D. & Huck, I.W., 1990. The structural history of a transtensional basin: Inner Moray Firth, NE Scotland, *J. geol. Soc.,* **147**(1), 87–103.

Rude, P.D. & Aller, R.C., 1989. Early diagenetic alteration of lateritic particle coatings in Amazon continental shelf sediment, *J. Sediment. Res.,* **59**(5), 704–716.

Schwertmann, U. & Fechter, H., 1984. The influence of aluminum on iron oxides: XI. aluminum-substituted maghemite in soils and its formation, *Soil Sci. Soc. Am. J.,* **48**(6), 1462–1463.

Song, X. & Boily, J.F., 2016. Surface and bulk thermal dehydroxylation of FeOOH polymorphs, *J. Phys. Chem. A,* **120**(31), 6249–6257.

Stevens, V., 1991. The Beatrice Field, Block 11/30a, UK North Sea, *Geol.l Soc. Lond. Memoirs,* **14**(1), 245–252.

Thiel, J., Byrne, J.M., Kappler, A., Schink, B. & Pester, M., 2019. Pyrite formation from FeS and H_2S is mediated through microbial redox activity, *Proc. Natl. Acad. Sci. U. S. A.,* **116**(14), 6897–6902.

Thomson, K. & Hillis, R.R., 1995. Tertiary structuration and erosion of the Inner Moray Firth, in *The Tectonics, Sedimentation and Palaeoceanography of the North Atlantic Region,* pp. 249–269, eds Scrutton, R.A., Stoker, M.S., Shimmield, G.B. & Tudhope, A.W, eds., Geological Society Special Publications.

Till, J.L. & Nowaczyk, N., 2018. Authigenic magnetite formation from goethite and hematite and chemical remanent magnetization acquisition, *Geophys. J. Int.,* **213**(3), 1818–1831.

Underhill, J.R. & Partington, M.A., 1993. Jurassic thermal doming and deflation in the North Sea: implications of the sequence stratigraphic evidence, *Geol. Soc., Lond., Petrol. Geol. Conf. Ser.,* **4,** 337–345.

Underhill, J.R., 1991. Implications of Mesozoic-Recent basin development in the western Inner Moray Firth, UK, *Mar. Petrol. Geol.,* **8,** 359–369.

van der Zee, C., Roberts, D.R., Rancourt, D.G. & Slomp, C.P., 2003. Nanogoethite is the dominant reactive oxyhydroxide phase in lake and marine sediments, *Geology,* **31**(11), 993–996.

Vandenberghe, R.E. & de Grave, E., 2013. Application of Mössbauer spectroscopy in Earth Sciences, in *Mössbauer Spectroscopy,* eds Yoshida, Y. & Langouche, G., Springer Verlag.

Vandenberghe, R.E., de Grave, E., de Greyler, G. & Landuydt, C., 1986. Characterization of goethite and hematite in a Tunisian soil profile by Mössbauer spectroscopy, *Clays Clay Miner.,* **34**(3), 275–280.

Verwey, E.J. W., 1939. Electronic conduction of magnetite (Fe_3O_4) and its transition point at low temperatures, *Nature,* **144**(3642), 327–328.

Weibel, R., 1999. Pseudomorphous transformation of goethite needles into hematite in sediments of the triassic skagerrak formation, Denmark, *Clay Miner.,* **34**(4), 657–660.

Whitbread, K. & Kearsey, T., 2016. Devonian and carboniferous stratigraphical correlation and interpretation in the orcadian area, central north sea, quadrants 7–22, Energy and Marine Geoscience Programme Commissioned Report CR/16/032, British Geological Survey, Keyworth, Nottingham.

Yamazaki, T., 2008. Magnetostatic interactions in deep-sea sediments inferred from first-order reversal curve diagrams: Implications for relative paleointensity normalization, *Geochem., Geophys., Geosyst.,* **9**(2), doi:10.1029/2007GC001797.